



Article citation info:

Xie J, Tian Z, Zhi P, Zhao Y, Reliability analysis method of coupling optimal importance sampling density and multi-fidelity Kriging model. *Eksplloatacja i Niezawodność – Maintenance and Reliability* 2023; 25(2) <http://doi.org/10.17531/ein/161893>

Reliability analysis method of coupling optimal importance sampling density and multi-fidelity Kriging model

Indexed by:


Jiayu Xie^a, Zongrui Tian^b, Pengpeng Zhi^{c,d,e*}, Yadong Zhao^{b,f}

^a Aeronautical Engineering College, Civil Aviation Flight University of China, Guanghan 618307, Sichuan, China

^b Anyang Key Laboratory of Advanced Aeronautical Materials and Processing Technology, Anyang Institute of Technology, Anyang 455099, China

^c Yangtze Delta Region Institute (Huzhou), University of Electronic Science and Technology of China, Huzhou 313001, Zhejiang, China

^d Institute of Electronic and Information Engineering in Guangdong, University of Electronic Science and Technology of China, Dongguan 523808, Guangdong, China

^e School of Mechanical and Electrical Engineering, University of Electronic Science and Technology of China, Chengdu 611731, Sichuan, China

^f School of Mechanical Engineering, Anyang Institute of Technology, Anyang 455099, China

Highlights

- Proposed a learning function for multi-fidelity models.
- A practical reliability calculation stopping condition is proposed.
- Proposed a feasible and applicable structural reliability analysis framework for multi-fidelity models.

Abstract

The commonly used reliability analysis approaches for Kriging-based models are usually conducted based on high-fidelity Kriging models. However, high-fidelity surrogate models are commonly costly. Therefore, in order to balance the calculation expense and calculation time of the surrogate model, this paper proposes a multi-fidelity Kriging model reliability analysis approach with coupled optimal important sampling density (OISD+MFK). First, the MEI learning function is proposed considering the training sample distance, model computation cost, expected improvement function, and model relevance. Second, a dynamic stopping condition is proposed that takes into account the failure probability estimation error. Finally, the optimal importance sampling density is incorporated into the reliability analysis process, which can effectively reduce failure probability estimation error. The results of the study show that the approach proposed in this paper can reduce the calculation cost while outputting relatively accurate failure probability evaluation results.

Keywords

reliability analysis, multifidelity model, learning function, stopping condition

This is an open access article under the CC BY license (<https://creativecommons.org/licenses/by/4.0/>) 

1. Introduction

The influence of uncertainties such as structural parameters and load randomness in the manufacturing process of engineering structures makes structural reliability analysis crucial for structural performance assessment. The probability of failure is a key indicator of reliability analysis, which can calculate the probability that a structure does not meet the requirements of use. It can be mathematically described as

$$P_f = \int_{G(x) \leq 0} f(x) dx \quad (1)$$

where P_f is the failure probability, $x=(x_1, x_2, \dots, x_n)$ is random variables, $G(x)$ is the limit state function (LSF), $f(x)$ is the joint probability density function of random variables.

In large-scale engineering applications, the LSF is usually a high-dimensional nonlinear black-box function, so it is very difficult to solve. The approximation methods for solving the function have been developed, including the first-order/second-order method [1-2], line sampling method [3], directional

(*) Corresponding author.
E-mail addresses:

J. Xie (ORCID: 0000-0002-4790-8265) xiejiayu1983@gmail.com, Z. Tian (ORCID: 0000-0001-7225-1050) tianzongrui9731@163.com, P. Zhi (ORCID: 0000-0003-1537-8455) zhipeng17@yeah.net, Y. Zhao (ORCID: 0000-0002-3774-1289) zhaoyd@ayit.edu.cn

sampling method [4], importance sampling method [5], Monte Carlo method [6], cross-entropy method [7], and subset simulation [8]. However, if the limit state function contains multiple failure domains or has nonlinear characteristics, the results of the above methods will obtain a failure probability with an unsatisfactory accuracy. Therefore, a large number of simulations of the LSF are required to obtain results with high accuracy. For example, in MCS, the failure probability expression is

$$P_f = \int f(x)I(x) dx \approx \frac{1}{N_{MCS}} \sum_{i=1}^{N_{MCS}} I(x_i) \quad (2)$$

where $I(x)$ is the indicator function with the property that $I(x) = 1$ when $G(x) \leq 0$, N_{MCS} is the number of Monte Carlo samples and x_i is the i th sample in the N_{MCS} .

However, with the flying advancement of PC engineering, the degree of refinement of reliability analysis models is increasing, and the evaluation cost of limit state functions is gradually increasing. To reduce the total calculation expense, the implementation of surrogate models in the framework of structural reliability analysis is an effective approach. The commonly used surrogate models, including the Kriging model [9-11], radial basis function (RBF) model [12], the response surface model (RSM) [13,14], the polynomial chaos expansion (PCE) model [15-17], and the support vector regression (SVR) model [18,19]. These surrogate models are able to fit the characteristics of the real LSF by a sample set. Since the kriging model can obtain the standard deviation of the test samples, it can be broadly used in the domain of reliability assessment. The Kriging model can calculate reliability in two ways, the first is to build a static Kriging model to calculate reliability, and the second is to integrate the active learning process into the Kriging model-building process, while dynamically updating reliability. In most cases, the second approach is more efficient than the first one.

Some scholars have exploited the characteristic of kriging models that can quantify uncertainty information to make accurate predictions of limit states. For example, Bichon et al. [20] proposed the Efficient Global Reliability Analysis (EGRA) algorithm, which proposes the Expectation Feasibility Function (EFF) to candidate samples that are approaching limit states. Echard et al. [21] proposed a new practical approach by combining Kriging and MCS (AK-MCS), which introduced the

currently popular learning function U. Jones et al. [22] implements global optimization of black-box functions by using the Expected Improvement Function (EIF). Zhi et al. [23] proposed a γ_U function based on the U function, which further optimized the sampling characteristics of the U function. Xiao et al. [24] proposed a new learning function with parallel processing strategy.

Afterward, the learning function H [25] evaluates the uncertainty of the sample using information entropy theory. Sun et al. [26] proposed the Least Improvement Function (LIF), which integrates the uncertainty and probability density function for improving the failure probability, but its application is limited by its complex expressions. Zhang et al. [27] developed a reliability-based expectation improvement function REIF and an improved version REIF2 by using a folded normal distribution.

The stopping condition of the active learning process is also an essential element that influences the accuracy and efficiency of the reliability results. The conventional stopping condition is usually established as a constant, which is derived from the calculation of the learning function. The iterative procedure halts when the result of the learning function reaches a threshold value. Considering that the conventional stopping conditions may not satisfy the accuracy of the failure probability prediction, the thresholds used are more stringent. Therefore, to improve the universality of termination conditions, Hu and Mahadevan [28] established the relative error estimates between the true and evaluated failure probabilities. Wang et al. [29] considered the uncertainty of the Kriging model and then evaluated the maximum relative error of the failure probability in accordance with the error stopping criterion (ESC). To improve the efficiency of ESC, Yi et al. [30] introduced a new ESC which focuses on highly uncertain samples. The results show that ESC demonstrates better superiority in the active learning process.

However, for most methods, the data used for surrogate model construction are obtained from high-fidelity (HF) models. High-fidelity models usually require expensive simulations for simulation, thus restricting the total number of available runs. As a result, models with multiple fidelities have gradually become a hot research topic. Although the uncertainty of low-fidelity (LF) is larger than that of high-fidelity models,

it can provide valid model information and has a much lower calculation cost than high-fidelity models, which indicates that low-fidelity models have good prospects for development. The multi-fidelity (MF) model combines the advantages of both HF and LF models and thus a sound balance between evaluation error and cost can be provided. Qian and Wu [31] explored a hierarchical Gaussian process model for treating HF and LF data simultaneously. Zhou et al. [32] developed a robust optimization method based on a multi-fidelity surrogate model, which takes into account the uncertainty of the surrogate model and design variables. Chaudhuri et al. [33] proposed the multi-fidelity EGRA (mfEGRA) method to solve the problem of reliability analysis of multi-fidelity data. Lefebvre et al. [34] evaluated the failure probability of industrial assemblies using Co-Kriging, and the results had reasonable computational cost and acceptable accuracy. Cheng et al. [35] introduced a variable-fidelity constrained lower confidence bound (VF-CLCB) criterion to address the expensive function-constrained optimization problem. At present, the Co-Kriging variable confidence approximation model is less used in structural reliability analysis.

At present, multi-fidelity kriging models are widely used in the fields of optimization and regression analysis but rarely applied to structural reliability analysis. Therefore, aiming at the reliability analysis of multi-fidelity data, this paper proposes a reliability analysis method for multi-fidelity models with coupled optimal important sampling density. The method can be used to obtain accurate reliability estimation by multi-fidelity kriging model and active learning process of optimal importance sampling technique.

The contributions of the proposed research work can be summarized as follows

(1) A new learning function construction method is proposed, which is a new method capable of selecting the optimal fit sample from a candidate sample set. It can consider the computational cost of both HF and LF models, as well as the crowding distance of the training samples and the approximation to the LSF. The characteristics of the model can be captured more effectively by considering the fitting performance of the model.

(2) A new stopping condition is proposed which stops the point addition process based on the estimated value of the

relative error.

(3) The optimal important sampling density is implemented in the reliability analysis process to effectively improve the speed of failure probability assessment.

The rest of the paper is divided into 5 sections. Section 2 retrospects the basic principles of Co-Kriging, a method for calculating the probability of failure using the optimal importance sampling density, and the classic expected improvement function. Section 3 mainly describes the innovation points of the proposed method. Section 4 describes the steps of the computational process of the proposed method. Section 5 demonstrates the advantages of the method with several application examples. The conclusions obtained in this paper are described in Section 6.

2 Fundamental background

2.1 Basic concept of the Co-Kriging model

According to the reference [36], as a variable fidelity approximation model, Co-Kriging can provide information about the prediction error at non-sample points, which can be easier to fit the LSF in the reliability problem. To construct the Co-Kriging approximation model, two sets of sample data with different fidelity levels are required, where the high fidelity expensive sample points and response values are denoted as X_h and Y_h , and the low confidence sample points and response values are denoted as X_l and Y_l , respectively. The two sets of high and low fidelity sample points are independent of each other, and there are n_h high fidelity sample points and n_l low fidelity sample points. In general, the high fidelity sample size is smaller than the low fidelity sample size, and the two part sample points and output response values are as follows

$$X=(X_l, X_h)^T=(x_l^1, \dots, x_l^{n_l}, x_h^1, \dots, x_h^{n_h})^T \quad (3)$$

$$Y=(Y_l, Y_h)^T=(Y_l(x_l^1), \dots, Y_l(x_l^{n_l}), Y_h(x_h^1), \dots, Y_h(x_h^{n_h}))^T \quad (4)$$

The expression for the approximate estimate of the Co-Kriging surrogate model is as follows

$$Z_h(x)=\rho Z_l(x)+Z_\delta(x) \quad (5)$$

where ρ is a scalar coefficient, Z_l denotes the model consisting of low confidence samples, and Z_δ denotes the model consisting of the difference between high and low confidence samples. Similar to the Kriging model approach, the covariance matrix of the Co-Kriging model is constructed as follows

$$c = \begin{pmatrix} \sigma_l^2 R_l(X_l, X_l) & \rho \sigma_l^2 R_l(X_l, X_h) \\ \rho \sigma_l^2 R_l(X_h, X_l) & \rho \sigma_l^2 R_l(X_h, X_h) + \sigma_d^2 R_d(X_h, X_h) \end{pmatrix} \quad (6)$$

where R_l and R_d represent the spatial correlation matrices of the models corresponding to different sample data X_l and X_h , respectively, σ_c represents the standard deviation of the low confidence approximation model, and σ_d represents the standard deviation of the difference model, which can be calculated by maximum likelihood estimation. Because there are two correlation matrices R_l and R_d in the building of Co-Kriging approximation model, there are correlation parameters that need to be estimated θ_l and θ_d as well as the amplification factor ρ . Since the data at the high and low confidence sample points are independent of each other, the parameter estimation approach for the low confidence model can be referred to the Kriging model. For the parameters of the difference model, the expression is defined as

$$y_d = y_h - \rho y_l(X_h) \quad (7)$$

where $y_l(X_h)$ represents the value of the point X_h in the low-confidence model. In this way, the parameters for the different models can also be derived using an optimization procedure similar to Kriging.

The predicted mean and variance of Co-Kriging are expressed respectively as

$$y_h(x) = \mu + c^T C^{-1} (Y - 1\mu) \quad (8)$$

$$s_h^2(x) = \rho^2 \sigma_l^2 + \sigma_d^2 - c^T C^{-1} c \quad (9)$$

where, x indicates the input variable, $\mu = \frac{1^T C^{-1} Y}{1^T C^{-1} 1}$, $\mathbf{1}$ is an n -dimensional column vector consisting of 1. The expression of the vector c is

$$c = \begin{pmatrix} \rho \sigma_l^2 R_l(X_l, x) \\ \rho^2 \sigma_l^2 R_l(X_h, x) + \sigma_d^2 R_d(X_h, x) \end{pmatrix} \quad (10)$$

2.2 Failure Probability Based on Optimal Importance Sampling Density

To minimize the error in the predicted value of the probability of failure \hat{P}_f , a theoretically optimal important sampling density function $h_{opt}(x)$ can be derived, whose expression is as follows

$$h_{opt}(x) = \frac{I_f(x) f_x(x)}{P_f} \quad (11)$$

where P_f represents the true value of the failure probability. Since the P_f is only an unknown quantity to be estimated, it is obviously impractical to solve $h_{opt}(x)$ precisely. However, the Kriging model of LSF $g_k(x)$ is used to construct the current

significant sampling density function $h_x(x)$, defined as

$$h_x(x) = \frac{\pi(x) f_x(x)}{P_{f_e}} \quad (12)$$

where $\pi(x)$ represents the probability of $g_k(x) \leq 0$ at the sample point x obtained from the current Kriging model $g_k(x)$, defined as follows:

$$\pi(x) = P\{g_k(x) \leq 0\} = \Phi\left(-\frac{\mu_{g_k}(x)}{\sigma_{g_k}(x)}\right) \quad (13)$$

where $g_k(x)$ follows a normal distribution $g_k(x) \sim N(\mu_{g_k}(x), \sigma_{g_k}^2(x))$, $\mu_{g_k}(x)$ and $\sigma_{g_k}^2(x)$ are the predicted mean and predicted standard deviation of $g_k(x)$, respectively. When $g_k(x)$ can replace $g(x)$ very accurately, $\pi(x)$ will be close to $I_f(x)$.

P_{f_e} is the normalization factor and is defined as follows:

$$P_{f_e} = \int \cdots \int_{R^n} \pi(x) f_x(x) dx \quad (14)$$

where P_{f_e} is also known as the augmented failure probability. Adopting the importance sampling density function $h_x(x)$ constructed by the Kriging model, the following derivation can be made for the estimator of the failure probability.

$$P_f = P_{f_e} \alpha_{corr} \quad (15)$$

where $\alpha_{corr} = \int \cdots \int_{R^n} \frac{I_f(x)}{\pi(x)} h_x(x) dx$ is called the correction factor.

2.3 Expected Improvement Function

The EIF is mainly applied in the field of global optimization. It determines the choice of each update point and the search direction of the global algorithm. The degree of improvement is reflected in the concept known as expected improvement, defined as

$$EI = (f_{\min} - \hat{y}(x)) \Phi\left(-\frac{f_{\min} - \hat{y}(x)}{\sigma_{\hat{y}}(x)}\right) + \sigma_{\hat{y}}(x) \phi\left(-\frac{f_{\min} - \hat{y}(x)}{\sigma_{\hat{y}}(x)}\right) \quad (16)$$

where f_{\min} is the minimum point sampled thus far, $\hat{y}(x)$ is the predicted output value at sample point x , $\sigma_{\hat{y}}(x)$ is the predicted standard deviation value at sample point x , Φ is the cumulative distribution function, and ϕ is the probability density function.

3 The proposed OISD+MFK method

In the field of adaptive reliability analysis, the selection of learning function and stopping conditions is crucial. For the learning function, it is possible to select suitable samples and add them to the experimental design, which in turn increases the number of fitted samples, and then corrects the model as fast as

possible during the continuous updating of the model. The candidate points of these samples are generally selected in the candidate set, which can be obtained by performing Monte Carlo sampling in the input space. The stopping condition is used to determine when to stop the adaptive sampling process. The stopping condition usually changes depending on the value of the learning function, and the modification of the model is stopped when the prediction accuracy is judged to be required in order to avoid the waste of computational cost.

3.1 MEI learning function

In order to further optimize the efficiency of screening samples in the active learning process, a learning function that can fully take into account the computing cost of different degrees of fidelity is established by extending the ordinary EI filling criterion by accounting for the correlation of different confidence levels, as well as the distance between training samples, defined as

$$MEI(x,t) = \begin{cases} VEI(x,t)d(x)r(x,t)CR(t) & ,t=l \\ VEI(x,t)d(x) & ,t=h \end{cases} \quad (17)$$

where $VEI(x,t)$ is a variant EI function built based on the EI function, t denotes the fidelity of the model, h denotes the HF model, and l denotes the LF model. $r(x,t)$, $d(x)$, and $CR(t)$ are the intercorrelation function, the sample distance, and the cost ratio function, respectively, and the key factors of these learning functions will be elaborated in the following subsections.

The MEI function is able to obtain sample points from data with different fidelities. According to the sampling characteristics of the MEI function, the location of the update points is obtained by maximizing the MEI function,

$$(x^*, t^*) = \operatorname{argmax} MEI(x,t), t=l, h \quad (18)$$

According to (18), each candidate sample corresponds to two update samples in the process of each iteration, which are built with HF and LF models, respectively, by filtering the maximum of which is the most optimal update point.

3.1.1 VEI learning function

The EI function is transformed so that it can be applied to the MF model with the expression as follows

$$VEI(x,t) = \begin{cases} (-\hat{y}_l(x)) \Phi\left(\frac{-\hat{y}_l(x)}{\sigma_{\hat{y}_l(x)}}\right) + \sigma_{\hat{y}_l(x)} \phi\left(\frac{-\hat{y}_l(x)}{\sigma_{\hat{y}_l(x)}}\right) - \hat{y}_l(x), t=l \\ (-\hat{y}_h(x)) \Phi\left(\frac{-\hat{y}_h(x)}{\sigma_{\hat{y}_h(x)}}\right) + \sigma_{\hat{y}_h(x)} \phi\left(\frac{-\hat{y}_h(x)}{\sigma_{\hat{y}_h(x)}}\right) - \hat{y}_h(x), t=h \end{cases} \quad (19)$$

where $\hat{y}_l(x)$ is the predicted mean value of the LF model, $\sigma_{\hat{y}_l(x)}$ is the predicted standard deviation of the LF model, $\hat{y}_h(x)$ is the predicted mean value of the HF model, and $\sigma_{\hat{y}_h(x)}$ is the predicted standard deviation of the HF model.

3.1.2 The correlation function

The prediction accuracy corresponding to various fidelity models will also be different. Therefore, it is important to quantify the correlation between the LF model and HF model. The higher the correlation, indicating that the predicted value of the LF model is closer to the true value. The correlation is mainly affected by the prediction standard deviation, which is expressed as

$$r(x,t) = \begin{cases} \frac{\sigma_{\hat{y}_l(x)}}{\sqrt{\sigma_{\hat{y}_l(x)}^2 + \sigma_{\hat{y}_h(x)}^2}} & ,t=l \\ 1 & ,t=h \end{cases} \quad (20)$$

3.1.3 Sample distance function

To consider the effect of sampling point distance with respect to the Kriging model and try to avoid the sample waste caused by too dense sampling points, for this reason, a sampling distance restriction function is introduced, whose expression is as follows

$$d(x) = \min \sqrt{(x - X_i)^2}, i=1, 2, \dots, n \quad (21)$$

where X_i is the i th training sample and n is the sample size of training samples.

3.1.4 Cost Ratio Function

To reasonably account for the difference in computation time for high/low accuracy models, the variable confidence MEI function introduces the cost ratio CR of high/low precision simulation models, which represents the cost ratio between conducting one high precision model simulation and conducting one low precision model simulation, i.e., the computational cost consumed by running one high precision simulation.

3.2 New Stopping Condition

As an important factor in active learning reliability analysis, the convergence criterion also affects the accuracy of calculation results. Setting a reasonable convergence criterion can ensure that the algorithm stops the calculation in time. At present, the more popular method is established based on the error of P_f . The error accuracy is evaluated to determine whether the algorithm stops or not. To further improve the computational efficiency of

the algorithm, the new convergence criterion proposed in this paper is established based on the error of P_f , which can ensure the adaptive convergence of the algorithm.

The relative error in estimating the P_f during active learning process is expressed as

$$\varepsilon_f = \frac{|P_f - \hat{P}_f|}{P_f} = \frac{|N_f - \hat{N}_f|}{N_f} \quad (22)$$

where N_f represents the sample size of true failure samples and \hat{N}_f represents the sample size of predicted failure samples.

As the number of active learning processes gradually increases, the error of P_f gradually decreases. And the number of failure sample symbol estimation errors is smaller than the number of total sample symbol estimation errors, so the relative error of P_f is expressed as

$$\varepsilon_f \leq \frac{S_{wrong}}{N_f} \quad (23)$$

where S_{wrong} represents the sample with wrong sign prediction among all samples.

Influenced by the effect of the approximation of the Kriging model, in this case, the judgment for the sign of the predicted sample is not necessarily accurate. In order to accurately define the sign of the predicted failure sample, the expression exists as follows

$$S_f = \{x | \hat{y}(x) \geq 0 \cap \hat{y}(x) - \alpha \sigma_{\hat{y}(x)} \leq 0, x \in S_{MC}\} \quad (24)$$

$$F_f = \{x | \hat{y}(x) < 0 \cap \hat{y}(x) + \alpha \sigma_{\hat{y}(x)} \leq 0, x \in S_{MC}\} \quad (25)$$

$$S_s = \{x | \hat{y}(x) \geq 0 \cap \hat{y}(x) - \alpha \sigma_{\hat{y}(x)} > 0, x \in S_{MC}\} \quad (26)$$

$$F_s = \{x | \hat{y}(x) < 0 \cap \hat{y}(x) + \alpha \sigma_{\hat{y}(x)} > 0, x \in S_{MC}\} \quad (27)$$

where S_f is the sample with incorrect sign prediction in the safety domain, F_f is the sample with correct sign prediction in the failure domain, S_s is the sample with correct sign prediction in the safety domain, F_s is the sample with incorrect sign prediction in the failure domain. α is the error factor, and the confidence interval reaches 95%, when $\alpha=1.96$.

Thus, the new expression for the convergence criterion ζ is defined as follows

$$\zeta = \frac{N_{S_f} + N_{F_s}}{N_{S_f} + N_{F_f}} \leq [\zeta] \quad (28)$$

where N_{S_f} is the sample size of the set S_f , N_{F_s} is the sample size of the set F_s , N_{F_f} is the sample size of the set F_f , and $[\zeta]$ represents the error threshold. In this paper, we take 0.5.

4 Implementation flow of OISD+MFK algorithm

In summary, the flowchart of the OISD+MFK algorithm based on the novel learning function and stopping condition is shown in Figure 1, and the specific steps are summarized as follows

Step 1: DoE initialization. Initial samples $x_{initial}$ are generated with Latin Hypercube Sampling. These samples are the LF samples. Randomly select samples from the LF samples as the HF samples.

Step 2: Construct the initial Co-Kriging model. Co-Kriging model are built using LF samples and HF samples.

Step 3: Generate candidate samples S_{MC} . Generate candidate samples S_{MC} through Monte Carlo sampling. Output the response values of Monte Carlo samples using the Co-Kriging model.

Step 4: Search for the new training sample (x^*, t^*) . The corresponding sample is selected as a new sample in the candidate sample set according to Equation (18).

Step 5: Evaluate the stopping condition ζ .

Step 5.1: Evaluate augmented failure probability \hat{P}_{f_e}

Step 5.2: Evaluate the correction factor $\hat{\alpha}_{corr}$

Step 5.3: Evaluate failure probability \hat{P}_f

Step 5.4: If the stopping condition ζ is not smaller than 0.05, go back to step 3 and add the additional sample to the DoE and repeat the above steps, setting the number of iterations $k=k+1$. If the convergence criterion is smaller than 0.05, output the failure probability estimate \hat{P}_f .

Step 6: Check the coefficient of variation $Cov_{\hat{P}_f}$. If the coefficient of variation $Cov_{\hat{P}_f}$ is not smaller than 0.05, go back to step 3 and expand the Monte Carlo candidate sample set S_{MC} . If the coefficient of variation $Cov_{\hat{P}_f}$ is smaller than 0.05, proceed to **Step 7**.

Step 7: End of method. Outputs \hat{P}_f and $Cov_{\hat{P}_f}$.

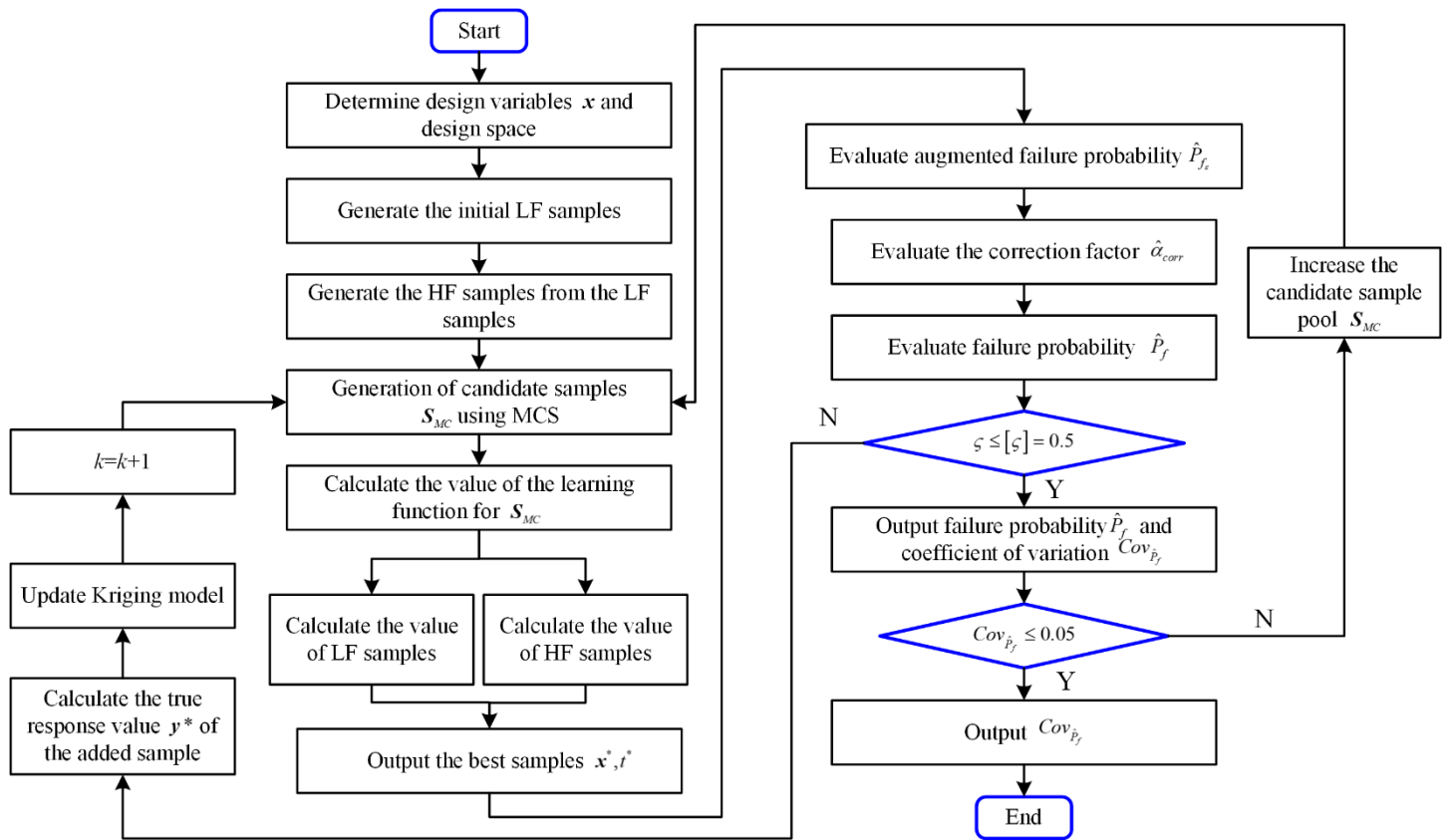


Fig. 1. Flow chart of OISD+MFK.

5 Illustration examples

In this section, two numerical cases and two engineering cases are used to conduct a comparative study of the OISD+MFK method and the commonly used methods to demonstrate the accuracy and effectiveness of the OISD+MFK method. The first example is a two-dimensional multimodal function, the second example is a four-branch tandem function, the third example is a cantilever beam, and the fourth example is a high-dimensional nonlinear vibration system. The comparison methods mainly include MCS, AK-MCS+U, and AK-MCS+EFF. To avoid randomness, each method was operated 30 times.

5.1 Example 1: Multimodal function

The first example of the algorithm is a two-dimensional highly nonlinear function, called a multimodal function. The expression of this function is as follows.

$$\begin{cases} G_1(\mathbf{x}) = 2 - \frac{(x_1^2 + 4)(x_2 - 1)}{20} - \sin\left(\frac{5x_1}{2}\right) \\ G_1(\mathbf{x}) = 2 - \frac{(x_1^2 + 4A)(x_2 - 1 - A)}{20} - \sin\left(\frac{5x_1}{2} - A\right) - \sin\left(\frac{5}{22}\left(x_1 + \frac{x_2}{2}\right) + \frac{5}{4}\right) \end{cases} \quad (29)$$

where the input variables x_1 follow the normal distribution

$N(1.5, 1)$, x_2 follow the normal distribution $N(2.5, 1)$, and are uncorrelated with each other. $A=0$, the cost ratio $CR=5$.

Figure 2 shows the adding point results and fitting performance of the multimodal function, where the black line indicates the actual limit state of the HF model, the green line indicates the actual limit state of the LF model, and the red dashed line indicates the predicted limit state. First, 20 LF samples and 6 HF samples are generated by LHS sampling. In Figure 2, LF samples are shown as pink solid dots and HF samples are shown as blue hollow hexagons. Using the MEI function to increase the training samples, 2 additional HF samples and 22 additional LF samples are generated, and in Fig. 2, the additional LF samples appear as pink solid pentagons and the additional HF samples appear as blue solid pentagons. From the location and sparsity of the samples, it can be seen that the additional training samples are located near the LSF, and thus are important for fitting the real LSF. Finally, by comparing the actual limit state curve and the predicted limit state curve, we can find that the two curves fit well in the global range.

Figure 3 shows the iteration history curve of MCS, AK-

MCS+U, AK-MCS+EFF, and OSID+MFK approaches to assess the failure probability. After 26 iterations, the algorithm reaches the stopping condition and the failure probability evaluation value gradually approaches the true P_f value as the number of iterations is updated.

The performance of the OSID+MFK method was compared with existing methods and the results of MCS, AK-MCS+EFF, and AK-MCS+U are presented in Table 1. As illustrated in Table 1, T_c is the computational cost of the combined LF and HF models. In terms of calculating cost, the T_c of OSID+MFK is 17.07, which has the smallest number of all methods. The T_c of AK-MCS+U

and AK-MCS+EFF are 41.46 and 55.82, respectively, which are significantly larger than that of OSID+MFK. For the accuracy results of the failure probability calculation, the OSID+MFK is 0.35%, which is somewhat bigger than the 0.32% of AK-MCS+EFF. Nevertheless, the calculated burden of AK-MCS+EFF is larger than that of OSID+MFK. In summary, the proposed OSID+MFK method has the optimal overall performance regarding computational accuracy and computational cost.

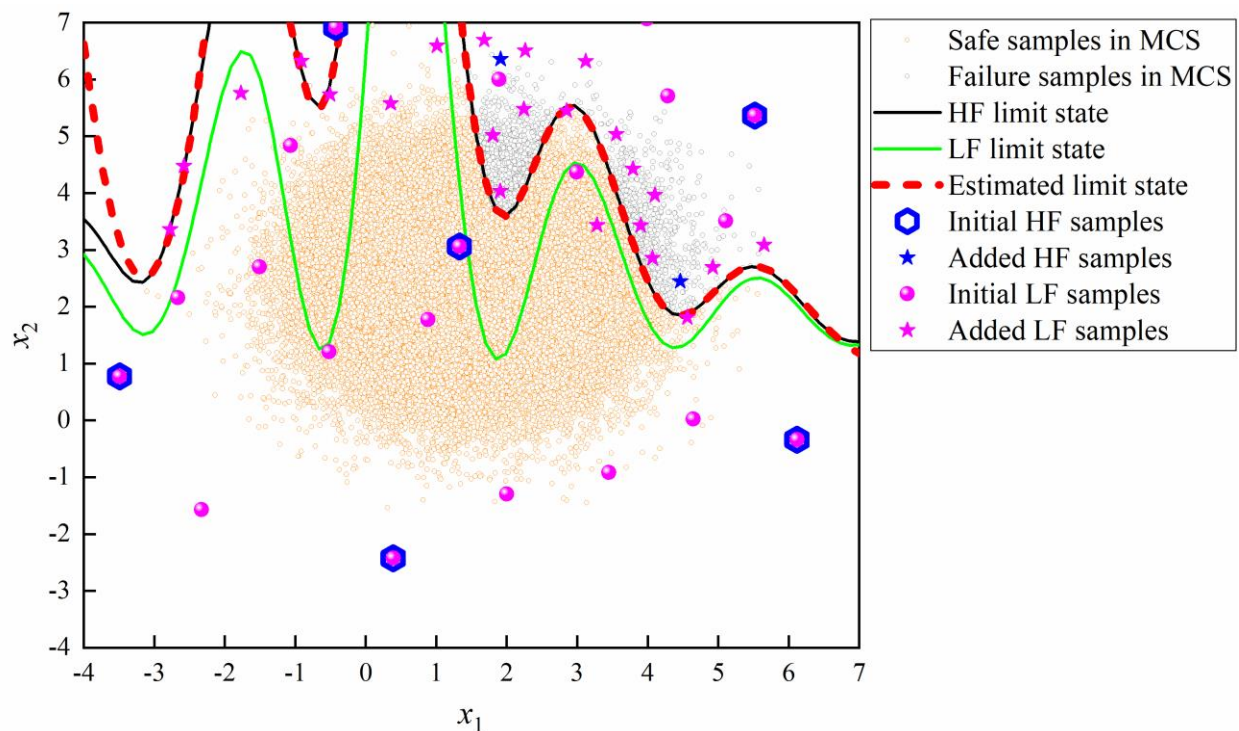


Fig. 2 Adding point results and fitting performance of OSID+MFK method for multimodal function.

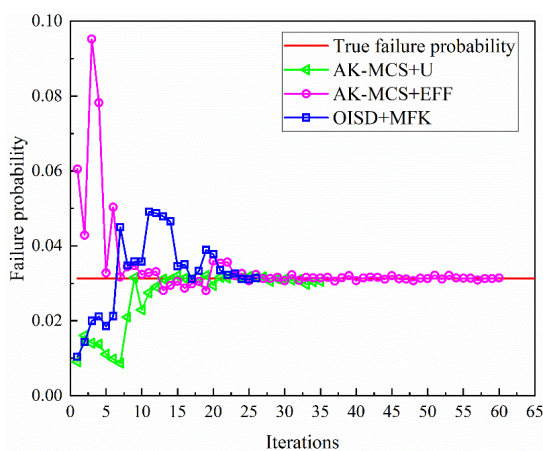


Fig. 3 Iterative curve of failure probability of MCS, AK-MCS+U, AK-MCS+EFF and OSID+MFK approaches for multimodal function.

Table 1 Reliability analysis results of MCS, AK-MCS+U, AK-MCS+EFF and OSID+MFK approaches for multimodal function.

| Methods | T_c | $\hat{P}_f (\times 10^{-2})$ | $Cov_{\hat{P}_f}$ (%) | $\varepsilon_{\hat{P}_f}$ (%) |
|------------|-------------------------|------------------------------|-----------------------|-------------------------------|
| MCS | 10^6 | 3.133 | 0.56 | - |
| AK-MCS+U | 41.46 | 3.111 | 0.56 | 0.70 |
| AK-MCS+EFF | 55.82 | 3.143 | 0.56 | 0.32 |
| OSID+MFK | $8.24+44.16 \times 0.2$ | 3.144 | 0.56 | 0.35 |

5.2 Example 2: Four branches series system

The second example is a four branches series function. The expression of the four-branch series function is as follows

$$\left\{ \begin{array}{l} G_h(\mathbf{x}) = \min \left\{ \begin{array}{l} 3 + \frac{(x_1 - x_2)^2}{10} - \frac{(x_1 - x_2)}{\sqrt{2}} \\ 3 + \frac{(x_1 - x_2)^2}{10} + \frac{(x_1 - x_2)}{\sqrt{2}} \\ (x_1 - x_2) + \frac{6}{\sqrt{2}} \\ (x_2 - x_1) + \frac{6}{\sqrt{2}} \end{array} \right. \\ \\ G_l(\mathbf{x}) = \min \left\{ \begin{array}{l} 3 + \frac{(x_1 - Ax_2)^2}{10} - \frac{(Ax_1 + x_2)}{\sqrt{2}} \\ 3 + \frac{(x_1 - Ax_2)^2}{10} + \frac{(Ax_1 + x_2)}{\sqrt{2}} \\ (x_1 - 0.9x_2) + \frac{7}{\sqrt{2}} \\ (x_2 - 0.9x_1) + \frac{7}{\sqrt{2}} \end{array} \right. \end{array} \right. \quad (30)$$

where the input variables x_1 and x_2 obey a standard normal distribution and are uncorrelated with each other. $A=1$, the cost ratio $CR=5$.

This function has more complexity than the last function

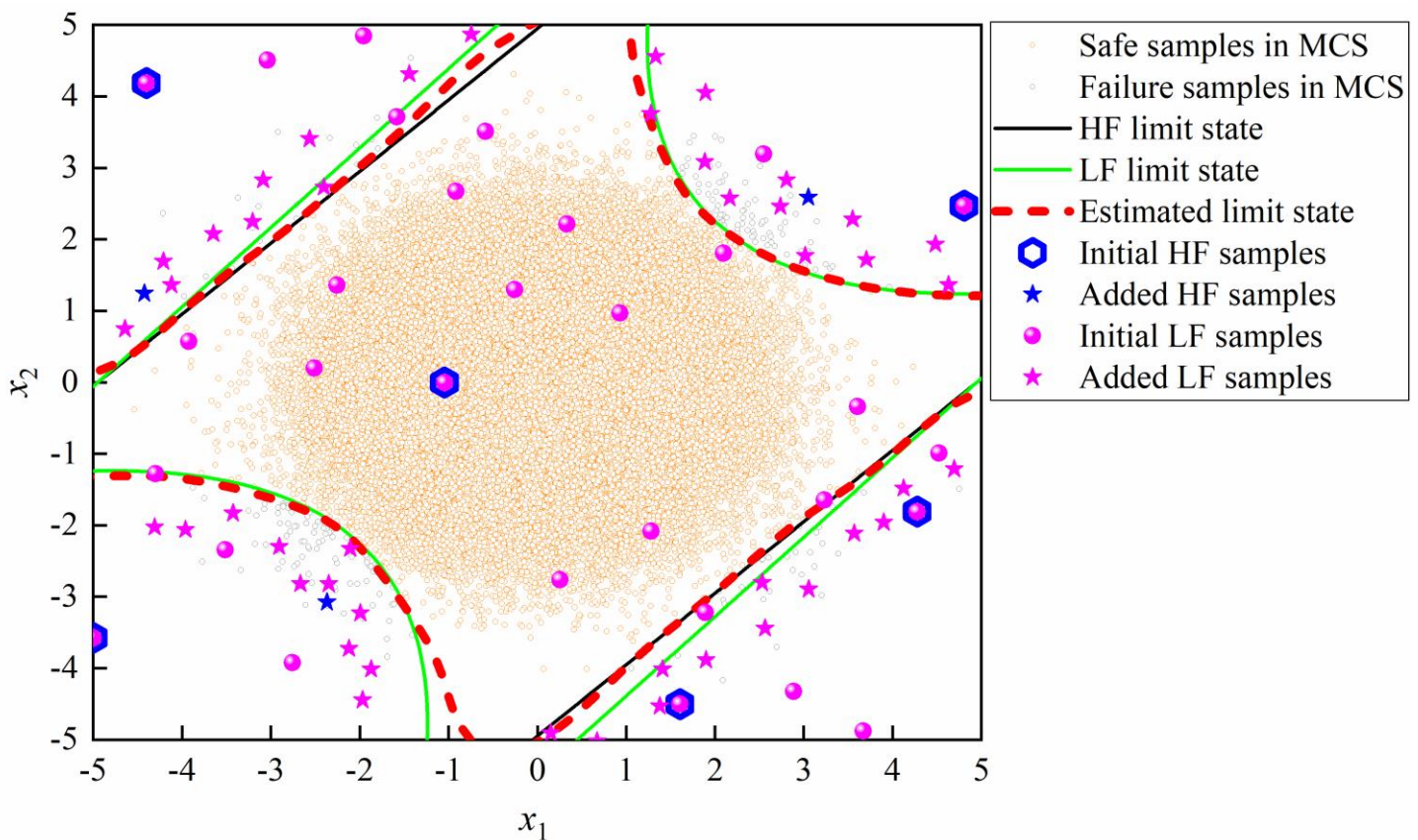


Fig. 4 Adding point results and fitting performance of OSID+MFK method for four branches series function.

The performance of the OSID+MFK method was compared against existing methods and the results of MCS, AK-MCS+EFF, and AK-MCS+U are presented in Table 2. As shown in Table 2, the standard outcome is $P_f = 2.221 \times 10^{-3}$. The total computational cost shows that OSID+MFK has the least computational cost, which is reduced by 55.37% and 57.54% compared to AK-MCS+U and AK-MCS+EFF, respectively. In terms of P_f error

because the calculation results of this function are affected by the four nonlinear functions together.

Firstly, 30 LF samples and 6 HF samples were generated by LHS sampling. Figure 2 shows the final fitting results of the four-branch tandem function. It can be seen in the figure that the majority of the additional HF and LF samples are approaching the HF limit state function, and no invalid added samples are generated. It shows that the algorithm can effectively obtain meaningful samples near HF.

Figure 4 shows the iteration history curve of the OSID+MFK method to evaluate the reliability. After 48 iterations, the algorithm gradually smoothed out and reached the stopping condition.

results, the failure errors of AK-MCS+U, AK-MCS+EFF, and OSID+MFK are 4.68%, 1.35%, and 0.45%, respectively. the error results of OSID+MFK are the smallest, thus it can be seen that the OSID+MFK method shows good competitiveness with regard to both the calculation cost and the accuracy of the P_f calculation.

Table 2 Reliability analysis results of MCS, AK-MCS+U, AK-MCS+EFF and OISD+MFK approaches for four branches series function.

| Methods | T_c | $\hat{P}_f (\times 10^{-3})$ | $Cov_{\hat{P}_f}$ (%) | $\varepsilon_{\hat{P}_f}$ (%) |
|------------|-------------------------|------------------------------|-----------------------|-------------------------------|
| MCS | 10^7 | 2.221 | 0.67 | - |
| AK-MCS+U | 54.56 | 2.325 | 0.66 | 4.68 |
| AK-MCS+EFF | 57.35 | 2.251 | 0.67 | 1.35 |
| OISD+MFK | $9.26+75.43 \times 0.2$ | 2.211 | 0.67 | 0.45 |

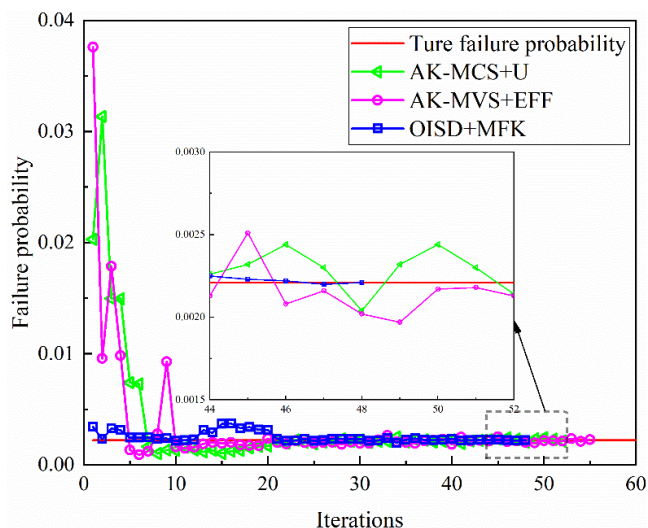
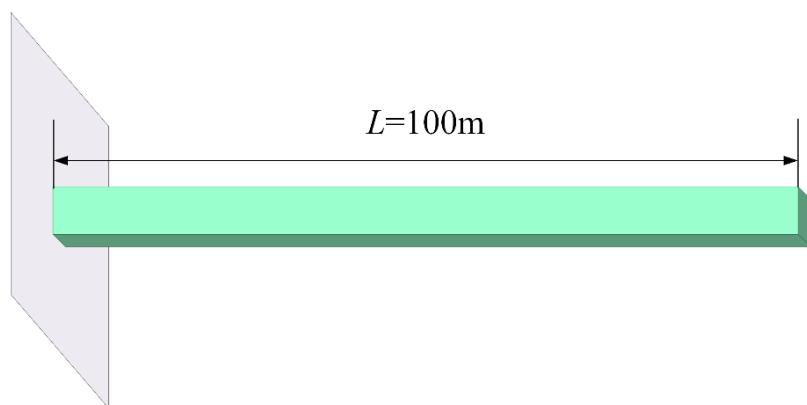


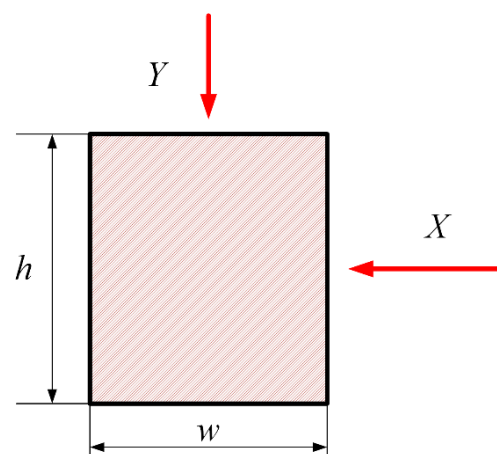
Fig. 5 Iterative curve of failure probability of OISD+MFK approach for four branches series function.

5.3 Example 3: An cantilever beam

The third example is studied with a cantilever beam of a rectangular section. The schematic diagram of the cantilever beam is shown in Fig. 6(a). The cantilever beam is burdened with loads in horizontal and vertical directions, and the force diagram



(a)



(b)

Fig. 6 Cantilever beam structure (a) Schematic diagram of cantilever beam (b) Cross-section force diagram.

of its cross-section is shown in Fig. 6(b). The LSF of the force state of the cantilever beam is established with its free end displacement not exceeding ΔD as a constraint, and the specific mathematical expressions are as follows.

$$\begin{cases} F_h(E,X,Y,w,t,L)=\Delta D-D_{max}=2.2-\frac{4L^3}{Ewt}\sqrt{\left(\frac{X}{w^2}\right)^2+\left(\frac{Y}{t^2}\right)^2} \\ F_l(E,X,Y,w,t,L)=2.2-\frac{4L^3}{Ewt}\sqrt{\left(\frac{X+0.01}{w^2}\right)^2+\left(\frac{Y+0.1}{t^2}\right)^2} \end{cases} \quad (31)$$

where ΔD is the free end displacement threshold, D_{max} is the maximum free end displacement, E is the modulus of elasticity of the material, w is the width of the beam, t is the beam height, L is the beam length, and the cost ratio $CR=2$. ΔD , w , t , and L are constants, and their specific values are shown in Table 3. X and Y are normal distributed variables, and their parameters are shown in Table 4.

Table 3 Constant parameters of cantilever beam structure.

| Constant | value |
|----------------------|--------|
| $\Delta D/\text{mm}$ | 2.2 |
| w/m | 2.4884 |
| t/m | 3.8884 |
| L/m | 100 |

Table 4 Variable parameters of the cantilever beam structure.

| Random variable | Distribution | Mean | Standard deviation |
|-----------------|--------------|-------------------|--------------------|
| X/N | Normal | 500 | 100 |
| Y/N | Normal | 1000 | 100 |
| E/Pa | Normal | 2.9×10^7 | 1.45×10^6 |

Table 5 Reliability analysis results of MCS, AK-MCS+U, AK-MCS+EFF and OISD+MFK approaches for cantilever beam structure.

| Methods | T_c | $\hat{P}_f (\times 10^{-3})$ | $Cov_{\hat{P}_f}$ (%) | $\varepsilon_{\hat{P}_f}$ (%) |
|------------|----------------------|------------------------------|-----------------------|-------------------------------|
| MCS | 10^6 | 2.711 | 1.92 | - |
| AK-MCS+U | 26.23 | 2.683 | 1.93 | 1.03 |
| AK-MCS+EFF | 22.95 | 2.732 | 1.91 | 0.77 |
| OISD+MFK | $6+13.49 \times 0.5$ | 2.708 | 1.92 | 0.11 |

The initial HF samples were set with 6 and LF samples with 10. The MCS, AK-MCS+U, AK-MCS+EFF, and OISD+MFK methods were used for comparison and calculation, respectively. The results of all methods are given in Table 5.

It is found that the computational costs of MCS, AK-MCS+U, AK-MCS+EFF and OISD+MFK are 10^6 , 26.23, 22.95 and 12.75, respectively. the computational cost of OISD+MFK is the least, which is reduced by 51.39% and 44.44% compared

to K-MCS+U and AK-MCS+EFF, respectively. Meanwhile, the results of P_f given in Table 5 show that P_f evaluation error of the OISD+MFK method is the smallest and closest to the standard result of MCS of 2.711×10^{-3} , which indicates that the OISD+MFK method has some guiding significance to improve the calculation accuracy. In conclusion, the reliability analysis of the cantilever beam structure shows that the OISD+MFK method has greater advantages in terms of computational cost and probability of failure assessment. Through this example, it is proved that the OISD+MFK method is efficient and successful.

5.4 Example 4: Nonlinear oscillator system

The nonlinear oscillatory system belongs to a high-dimensional nonlinear function, which is shown schematically in Figure 7. The LSF expression of the nonlinear oscillatory system is as follows

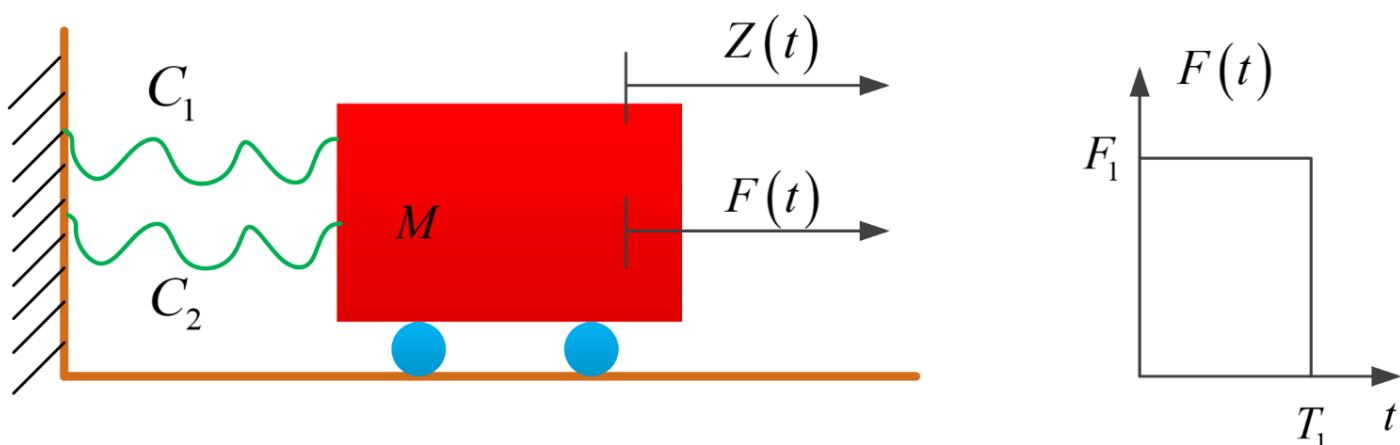


Fig. 7. The nonlinear oscillator system.

$$\begin{cases} G_h(C_1, C_2, M, R, T_1, F_1) = 3R - |Z_{max}| = 3R - \left| \frac{2F_1}{M\omega_0^2} \sin\left(\frac{\omega_0 T_1}{2}\right) \right| \\ G_l(C_1, C_2, M, R, T_1, F_1) = 3R - \left| \frac{2F_1}{M\omega_0^2} \sin\left(\frac{\omega_0 T_1}{2} - 0.1\right) \right| \end{cases} \quad (32)$$

where F_1 is the load, T_1 is the time course, M is the mass of the oscillator, C_1 and C_2 represent the two elasticity coefficients, R is the displacement of the system, ω_0 is the frequency of the system, Z_{max} is the maximum displacement of the system response, $3R$ is the maximum allowed displacement of the nonlinear restoring force, the cost ratio $CR=5$. The expression of ω_0 is as follows

$$\omega_0 = \sqrt{\frac{C_1 + C_2}{M}} \quad (33)$$

Table 6 The parameters of the nonlinear oscillator system.

| Random variable | Distribution | Mean | standard deviation |
|-----------------|--------------|------|--------------------|
| M | Normal | 1 | 0.05 |
| C_1 | Normal | 1 | 0.1 |
| C_2 | Normal | 0.1 | 0.01 |
| R | Normal | 0.5 | 0.05 |
| T_1 | Normal | 1 | 0.2 |
| F_1 | Normal | 1 | 0.2 |

Table 7 Reliability analysis results of MCS, AK-MCS+U, AK-MCS+EFF and OISD+MFK approaches for nonlinear oscillator system.

| Methods | T_c | \hat{P}_f ($\times 10^{-3}$) | Cov_{P_f} (%) | ε_{P_f} (%) |
|------------|--------------------------|-------------------------------------|--------------------|----------------------------|
| MCS | 10^6 | 2.432 | 2.05 | - |
| AK-MCS+U | 89.28 | 2.525 | 1.99 | 3.82 |
| AK-MCS+EFF | 105.46 | 2.489 | 2.00 | 2.34 |
| OISD+MFK | $11.15+75.43 \times 0.2$ | 2.500 | 2.00 | 2.80 |

In this algorithm, the initial Kriging model is created from 8 HF samples and 40 LF samples. The performance results of the OISD+MFK, MCS, AK-MCS+EFF and AK-MCS+U are presented in Table 7. As shown in Table 7, the standard outcome is $P_f = 2.221 \times 10^{-3}$. The corresponding T_c for AK-MCS+U and AK-MCS+EFF are 89.28 and 105.46, respectively, which are significantly bigger than the result of the OISD+MFK method. In addition, the relative errors of failure probabilities for these methods were 3.82%, 2.34%, and 2.80%, respectively. Although the error of the AK-MCS+EFF method is slightly larger than that of OISD+MFK, the calculation burden of this method is remarkably larger than that of the OISD+MFK method.

Consequently, in comparison with other methods, the OISD+MFK method can obtain satisfactory error accuracy with less calculation cost. This example shows that for the reliability problem of high-dimensional complex nonlinear functions, the proposed OISD+MFK shows favorable merits with respect to calculation demands and evaluation accuracy.

6 Conclusion

To surmount the problem that traditional reliability analysis methods cannot address multi-fidelity data, this paper proposes a structural reliability analysis method coupled with the optimal

importance sampling density function. The method integrates the computational cost of HF and LF models and can obtain relatively accurate failure probability estimates at a low cost.

By considering the training sample distance, the correlation of between various fidelity models, and the calculating cost, additional samples of suitable fidelity are automatically found among the candidate samples. The proposed stopping condition is able to obtain more conservative error estimates by scaling the relative error estimates. Two numerical cases and two engineering cases are used to verify the feasibility of the OISD+MFK method, and the performance shows that the OISD+MFK method is able to balance the calculation cost and error accuracy of the failure probability calculation. To summarize, the integrated performance of OISD+MFK is obviously superior to other comparison methods.

The analysis of the four cases leads to some main observations: (1) The stopping condition proposed would be effective in raising the operational efficiency of the algorithm. (2) The learning function that considers the computational cost is important to reduce the computational burden while generating an effective agent model. (3) The integration of the most important sampling density function into the reliability analysis process can make the failure probability assessment value more approximate to the true solution.

The proposed method in this paper has shown good results in dealing with the static reliability of components. Besides, in future research, the method of this paper can be broadened to address the study of time-variant reliability analysis problems.

Acknowledgments

This research was funded by Guangdong Basic and Applied Basic Research Foundation (grant No. 2021A1515110308), Natural Science Foundation of Sichuan Province (grant No. 2022NSFSC1941).

References

1. Du X P, Hu Z. First order reliability method with truncated random variables. *Journal of Mechanical Design* 2012; 134: 091005 (1-9), <https://doi.org/10.1115/1.4007150>.
2. Papadimitriou D I, Mourelatos Z P, Hu Z. Reliability analysis using second-order saddlepoint approximation and mixture distributions. *Journal of Mechanical Design* 2019; 141(2): 021401, <https://doi.org/10.1115/1.4041370>.
3. Depina I, Le T M H, Fenton G, et al. Reliability analysis with Metamodel Line Sampling. *Structural Safety* 2016; 60: 1–15, <https://doi.org/10.1016/j.strusafe.2015.12.005>.
4. Nie J, Ellingwood B R. Directional methods for structural reliability analysis. *Structural Safety* 2000; 22(3): 233–49, [https://doi.org/10.1016/S0167-4730\(00\)00014-X](https://doi.org/10.1016/S0167-4730(00)00014-X).

5. Denny M. Introduction to importance sampling in rare-event simulations. *European Journal of Physics* 2001; 22(4): 403–11, <https://doi.org/10.1088/0143-0807/22/4/315>.
6. Tamimi S, Amadei B, Frangopol D M. Monte Carlo simulation of rock slope reliability. *Computers and Structures* 1989; 33: 1495–505, [https://doi.org/10.1016/0045-7949\(89\)90489-6](https://doi.org/10.1016/0045-7949(89)90489-6).
7. Da Silva A M L, Fernandez R A G, Singh C. Generating capacity reliability evaluation based on Monte Carlo simulation and cross-entropy methods. *IEEE Transactions on Power Systems* 2010; 25(1): 129-137, <https://doi.org/10.1109/TPWRS.2009.2036710>.
8. Papaioannou I, Betz W, Zwirgmaier K, et al. MCMC algorithms for subset simulation. *Probabilistic Engineering Mechanics* 2015; 41: 89-103, <https://doi.org/10.1016/j.proengmech.2015.06.006>.
9. Jiang C, Qiu H B, Gao L, et al. Real-time estimation error-guided active learning Kriging method for time-dependent reliability analysis. *Applied Mathematical Modelling* 2020; 77: 82-98, <https://doi.org/10.1016/j.apm.2019.06.035>.
10. Sacks J, Welch W J, Mitchell T J, et al. Design and analysis of computer experiments. *Statistical science* 1989; 4(4): 409-423, <https://doi.org/10.1214/ss/1177012413>.
11. Parnianifard A, Azfanizam A S, Ariffin M K A, et al. Crossing weighted uncertainty scenarios assisted distribution-free metamodel-based robust simulation optimization. *Engineering with Computers* 2020; 36: 139-150, <https://doi.org/10.1007/s00366-018-00690-0>.
12. Gutmann H M. A radial basis function method for global optimization. *Journal of global optimization* 2001; 19(3): 201-227, <https://doi.org/10.1023/A:1011255519438>.
13. Zheng Y, Das P K. Improved response surface method and its application to stiffened plate reliability analysis. *Engineering structures* 2000; 22(5): 544-551, [https://doi.org/10.1016/S0141-0296\(98\)00136-9](https://doi.org/10.1016/S0141-0296(98)00136-9).
14. Meng D B, Yang S Q, Zhang Y, et al. Structural reliability analysis and uncertainties-based collaborative design and optimization of turbine blades using surrogate model. *Fatigue & Fracture of Engineering Materials & Structures* 2019; 42(6): 1219-1227, <https://doi.org/10.1111/ffe.12906>.
15. Marelli S, Sudret B. An active-learning algorithm that combines sparse polynomial chaos expansions and bootstrap for structural reliability analysis. *Structural Safety* 2018; 75: 67–74, <https://doi.org/10.1016/j.strusafe.2018.06.003>.
16. Blatman G, Sudret B. Adaptive sparse polynomial chaos expansion based on least angle regression. *Journal of computational Physics* 2011; 230(6): 2345-2367, <https://doi.org/10.1016/j.jcp.2010.12.021>.
17. Torre E, Marelli S, Embrechts P, et al. Data-driven polynomial chaos expansion for machine learning regression. *Journal of Computational Physics* 2019; 388: 601-623, <https://doi.org/10.1016/j.jcp.2019.03.039>.
18. Smola A J, Schölkopf B. A tutorial on support vector regression. *Statistics and computing* 2004; 14(3): 199-222, <https://doi.org/10.1023/B:STCO.0000035301.49549.88>.
19. Leцерf M, Allaire D, Willcox K. Methodology for dynamic data-driven online flight capability estimation. *AIAA Journal* 2015; 53(10): 3073-3087, <https://doi.org/10.2514/1.J053893>.
20. Bichon B J, Eldred M S, Swiler L P, et al. Efficient global reliability analysis for nonlinear implicit performance functions. *AIAA journal* 2008; 46(10): 2459-2468, <https://doi.org/10.2514/1.34321>.
21. Echard B, Gayton N, Lemaire M. AK-MCS: an active learning reliability method combining Kriging and Monte Carlo simulation. *Structural Safety* 2011; 33(2): 145-154, <https://doi.org/10.1016/j.strusafe.2011.01.002>.
22. Jones D R, Schonlau M, Welch W J. Efficient global optimization of expensive black-box functions. *Journal of Global optimization* 1998; 13(4): 455-492, <https://doi.org/10.1023/A:1008306431147>.
23. Zhi P P, Yun G L, Wang Z L, et al. A Novel Reliability Analysis Approach under Multiple Failure Modes Using an Adaptive MGRP Model[J]. *Applied Sciences* 2022; 12(18): 8961, <https://doi.org/10.3390/app12188961>.
24. Xiao N C, Yuan K, Zhan H. System reliability analysis based on dependent Kriging predictions and parallel learning strategy. *Reliability Engineering & System Safety* 2022; 218: 108083, <https://doi.org/10.1016/j.res.2021.108083>.
25. Lv Z Y, Lu Z Z, Wang P. A new learning function for Kriging and its applications to solve reliability problems in engineering. *Computers & Mathematics with Applications* 2015; 70(5): 1182-1197, <https://doi.org/10.1016/j.camwa.2015.07.004>.
26. Sun Z L, Wang J, Li R, et al. LF: A new Kriging based learning function and its application to structural reliability analysis. *Reliability Engineering & System Safety* 2017; 157: 152-165, <https://doi.org/10.1016/j.res.2016.09.003>.
27. Zhang X F, Wang L, Sørensen J D. REIF: A novel active-learning function toward adaptive Kriging surrogate models for structural reliability analysis. *Reliability Engineering & System Safety* 2019; 185: 440–54, <https://doi.org/10.1016/j.res.2019.01.014>.
28. Hu Z, Mahadevan S. Global sensitivity analysis-enhanced surrogate (GSAS) modeling for reliability analysis. *Structural and Multidisciplinary Optimization* 2016; 53(3): 501-521, <https://doi.org/10.1007/s00158-015-1347-4>.
29. Wang Z Y, Shafieezadeh A. ESC: an efficient error-based stopping criterion for kriging-based reliability analysis methods. *Structural and Multidisciplinary Optimization* 2019; 59(5): 1621-1637, <https://doi.org/10.1007/s00158-018-2150-9>.
30. Yi J X, Zhou Q, Cheng Y S, et al. Efficient adaptive Kriging-based reliability analysis combining new learning function and error-based stopping criterion. *Structural and Multidisciplinary Optimization* 2020; 62: 2517–36, <https://doi.org/10.1007/s00158-020-02622-3>.
31. Qian P Z G, Wu C F J. Bayesian hierarchical modeling for integrating low-accuracy and high-accuracy experiments. *Technometrics* 2008; 50(2): 192–204, <https://doi.org/10.1198/004017008000000082>.
32. Zhou Q, Wang Y, Choi S-K, et al. A robust optimization approach based on multi-fidelity metamodel. *Structural and Multidisciplinary Optimization*. 2018; 57 (2): 775–97, <https://doi.org/10.1007/s00158-017-1783-4>.
33. Chaudhuri A, Marques A N, Willcox K. mfEGRA: Multifidelity efficient global reliability analysis through active learning for failure boundary location. *Structural and Multidisciplinary Optimization* 2021; 64(2): 797-811, <https://doi.org/10.1007/s00158-021-02892-5>.
34. Lefebvre J P, Dompierre B, Robert A, et al. Failure probability assessment using co-kriging surrogate models. *Procedia Engineering* 2015; 133: 622-630, <https://doi.org/10.1016/j.proeng.2015.12.640>.
35. Cheng J, Lin Q, Yi J X. An enhanced variable-fidelity optimization approach for constrained optimization problems and its parallelization. *Structural and Multidisciplinary Optimization* 2022; 65(7): 1-21, <https://doi.org/10.1007/s00158-022-03283-0>.
36. Forrester A I J, Sóbester A, Keane A J. Multi-fidelity optimization via surrogate modelling. *Proceedings of the royal society a: mathematical, physical and engineering sciences*, 2007; 463(2088): 3251-3269, <https://doi.org/10.1098/rspa.2007.1900>